ARTICLES

Recalibrated Double Many-Body Expansion Potential Energy Surface and Dynamics Calculations for HN_2

P. J. S. B. Caridade, L. A. Poveda, S. P. J. Rodrigues, and A. J. C. Varandas*

Departamento de Química, Universidade de Coimbra, 3004-535 Coimbra, Portugal

Received: October 20, 2006; In Final Form: December 19, 2006

A single-sheeted double many-body expansion potential energy surface is reported for the lowest doublet state of HN_2 by fitting additional multireference configuration interaction energies in the N···NH channel. A stratified analysis of the root-mean-squared error indicates an accuracy superior to that achieved for the previously reported form. Detailed dynamical tests are also performed for the N + NH reaction using both the quasi-classical trajectory method and the capture theory, and the results are compared with available empirical data. The vibrational resonances of the HN_2 metastable radical are also calculated and compared with previous theoretical predictions.

1. Introduction

Interest in N_xH_y systems has been increasing in recent years because of their key role in the nitrogen chemistry, both in the gas phase and in the gas−solid interface.[1] Specifically, HN_2 is a well-known intermediary in the NO pollutant combustion reduction[2−6] and in the noncatalytic radical mechanism that leads to ammonia formation.[7] In a recent publication, Dickinson et al.[8] stressed the importance of transport coefficients in H−N_2 binary mixtures to model hydrogen−air flames.

Although the HN_2 radical is recognized as a metastable species, it has apparently never been explicitly detected by spectroscopic methods. In fact, only Selgren et al.[9] reported results based on HN_2^+ neutralization beam studies in which they observed radiative transitions (wavelength range 2700−4500 Å) between $n = 3$ Rydberg state of $^2A'$ and $^2A''(\pi)$ using potassium targets. As claimed by the authors,[9] this may constitute the first spectroscopic detection of the radical, although no other studies confirmed their analysis. An intriguing aspect of the HN_2 radical is the long-standing discussion concerning its lifetime. Several theoretical results[10−16] have predicted hydrodinitrogen to be short-lived (10^{-8}−10^{-9}s), while kinetic models of the thermal selective noncatalytic reduction of NO by ammonia require it to have a long lifetime in order to rationalize the experimental results.[2,17,18] Quoting Gu et al.,[14] "harmony between kinetic modeling studies and experiment can be achieved by postulating a lifetime of 10^{-4} s for the HN_2 species", which is 4 orders of magnitude or so larger than the theoretical predictions. However, an ad hoc manipulation of the HN_2 lifetime may not be the proper solution as other groups[19] have alerted for missing reactions and chemical equilibria in the considered kinetic models, e.g., the fast dissociation/recombination process $HN_2 \rightleftharpoons H + N_2$.[3,5,20,21] Moreover, Selgren et al.[9] concluded that the HN_2 lifetime should be less than 0.5 μs.

To study this and other aspects related to the HN_2 radical, we have recently reported[15] a global single-sheeted DMBE (double many-body expansion) potential energy surface for the ground electronic doublet state of the title system ($^2A'$), hereafter denoted as DMBE I. This function has been calibrated from accurate multireference configuration interaction[22] (MRCI) energies using the aug-cc-pVQZ (AVQZ) basis set of Dunning,[23,24] which have been subsequently corrected semiempirically by using the DMBE-scaled external correlation (DMBE-SEC) method[25] to extrapolate to the complete basis set/complete configuration interaction limit. As for applications, the DMBE I potential energy surface has been employed[16] both in classical and in quantum studies of various unimolecular and bimolecular reactions, as well as to calculate H−N_2 transport and diffusion coefficients.[8] Although the accuracy of DMBE I is estimated to be 1.0 kcal mol^{-1}, a spurious barrier of 0.5 K has been detected after publication in its long-range component, a finding also reported by Dickinson et al.[8] Although this feature is unlikely to have any practical implications in reaction dynamics at temperatures of relevance in most physical and chemical processes, this may not be the case for low- and ultralow-temperature regimes. This prompted us to carry out further high level ab initio calculations for the N + NH channel with a view to improve the reliability of the fitted potential energy surface. Such a work will be described in section 2.

Experimentally, the rate constant of the N + NH exothermic reaction has been the subject of a single direct measurement by Hack et al.[26] It has also been studied[20,21,27−29] indirectly based on assumptions that may have introduced some arbitrariness on its temperature dependence and even on its value at room temperature. In a previous publication, we have presented a quasi-classical trajectory/statistical mechanics study of the N + NH $\rightleftharpoons$ N_2 + H reactive system using the DMBE I potential energy surface. Although a fortuitous coincidence has led to good agreement with the reported experimental data and even with the suggested $T^{0.5}$ temperature-dependence of the rate

* To whom correspondence should be addressed. E-mail: varandas@qtvs1.qui.uc.pt.

10.1021/jp066898h CCC: $37.00
Published on Web 02/01/2007

TABLE 1: Numerical Values of the Extended Hartree−Fock Energy [Eq 2] for DMBE II

coefficients	$P^{(1)}$	$P^{(2)}$	$P^{(3)}$, $P^{(4)}$	$P^{(5)}$, $P^{(6)}$	$P^{(7)}$
c_1/a_0^0	−2.901 588 28	−1.098 951 54	0.431 487 22	−0.013 935 43	0.616 249 70
c_2/a_0^{-1}	0.398 546 88	−1.691 062 40	−0.958 625 89	−0.000 249 07	−0.021 886 33
c_3/a_0^{-1}	2.949 338 42	3.363 170 27	−0.588 419 50	0.002 428 47	0.205 251 74
c_4/a_0^{-2}	−0.785 133 61	0.109 920 62	1.294 609 55	−0.004 348 43	0.028 776 63
c_5/a_0^{-2}	−1.805 006 77	−2.338 944 00	0.965 549 45	−0.002 216 30	−0.013 181 54
c_6/a_0^{-2}	1.977 498 83	1.502 760 65	1.113 699 17	0.005 328 74	0.070 513 09
c_7/a_0^{-2}	−0.270 977 07	0.635 668 28	0.149 987 92	−0.002 453 28	−0.070 773 06
c_8/a_0^{-3}	0.576 722 13	−1.126 376 32	−0.800 003 27		
c_9/a_0^{-3}	0.555 271 03	−1.492 426 02	−1.076 191 12		
c_{10}/a_0^{-3}	−0.425 519 37	−0.554 562 05	0.267 875 84		
c_{11}/a_0^{-3}	2.383 111 47	2.256 725 72	−0.828 188 77		
c_{12}/a_0^{-3}	−0.003 532 09	1.295 348 98	−0.142 703 47		
c_{13}/a_0^{-3}	0.203 568 71	1.744 085 93	−0.269 758 78		
c_{14}/a_0^{-4}	−0.113 629 41	−0.033 751 61	0.569 554 00		
c_{15}/a_0^{-4}	−1.074 225 42	−0.685 564 36	0.210 027 86		
c_{16}/a_0^{-4}	−0.828 833 83	−0.120 205 53	0.506 017 02		
c_{17}/a_0^{-4}	0.241 207 02	0.989 543 97	−0.045 875 53		
c_{18}/a_0^{-4}	0.437 999 69	0.661 715 09	0.690 593 05		
c_{19}/a_0^{-4}	0.481 111 76	1.159 640 05	−0.098 334 99		
c_{20}/a_0^{-4}	−1.552 643 96	0.959 925 22	0.324 562 37		
c_{21}/a_0^{-4}	0.272 168 68	0.352 080 58	0.226 417 65		
c_{22}/a_0^{-4}	0.401 736 31	−0.060 311 24	0.186 012 86		
c_{23}/a_0^{-5}	0.034 820 64	−0.179 620 09	−0.179 255 66		
c_{24}/a_0^{-5}	−0.400 953 42	−0.405 386 98	0.002 206 62		
c_{25}/a_0^{-5}	0.150 759 47	0.456 693 42	−0.206 272 51		
c_{26}/a_0^{-5}	−0.346 189 38	0.427 403 86	−0.304 101 04		
c_{27}/a_0^{-5}	−0.183 188 10	−0.225 345 93	−0.083 848 32		
c_{28}/a_0^{-5}	0.305 070 92	0.691 896 75	−0.266 729 95		
c_{29}/a_0^{-5}	0.186 753 91	0.573 507 23	0.300 287 07		
c_{30}/a_0^{-5}	−1.001 001 58	0.344 352 55	−0.413 445 58		
c_{31}/a_0^{-5}	−0.659 633 94	−0.585 796 51	−0.302 813 59		
c_{32}/a_0^{-5}	0.105 986 29	−0.184 173 02	0.178 569 70		
c_{33}/a_0^{-5}	0.628 547 41	−0.612 343 70	0.019 156 13		
c_{34}/a_0^{-5}	0.169 163 60	−0.031 711 54	0.005 676 97		
c_{35}/a_0^{-6}	0.010 375 97	0.015 044 39	0.047 488 43		
c_{36}/a_0^{-6}	−0.001 117 39	−0.107 277 43	−0.024 305 80		
c_{37}/a_0^{-6}	0.010 337 02	0.129 565 87	0.121 688 74		
c_{38}/a_0^{-6}	−0.122 499 87	0.093 287 84	0.104 910 31		
c_{39}/a_0^{-6}	0.374 731 74	−0.020 916 09	0.126 878 45		
c_{40}/a_0^{-6}	−0.196 457 00	0.163 390 23	0.127 806 71		
c_{41}/a_0^{-6}	−0.014 568 97	−0.008 612 88	−0.038 628 58		
c_{42}/a_0^{-6}	0.174 228 60	0.015 038 96	0.112 609 76		
c_{43}/a_0^{-6}	0.049 932 95	0.107 677 99	−0.122 180 07		
c_{44}/a_0^{-6}	−0.238 197 51	0.212 412 82	0.111 217 38		
c_{45}/a_0^{-6}	0.078 103 18	−0.048 879 50	0.113 881 44		
c_{46}/a_0^{-6}	−0.113 169 08	0.037 106 86	−0.190 092 28		
c_{47}/a_0^{-6}	0.127 816 42	−0.472 848 12	0.119 963 66		
c_{48}/a_0^{-6}	−0.082 634 50	−0.019 021 51	−0.030 468 20		
c_{49}/a_0^{-6}	0.011 584 95	0.069 469 68	0.185 566 16		
c_{50}/a_0^{-6}	0.126 005 04	−0.152 617 14	0.234 849 07		
$\gamma_1^{(j)}/a_0^{-1}$	1.58	0.10	1.60	0.29	0.69
$\gamma_2^{(j)}/a_0^{-1}$	1.16	1.33	−0.39, 1.33	1.27, 1.02	0.54
$\gamma_3^{(j)}/a_0^{-1}$	1.16	1.33	1.33, −0.39	1.02, 1.27	0.54
$R_1^{(j),\mathrm{ref}}/a_0$	1.85	2.55	1.90	7.461	4.80
$R_2^{(j),\mathrm{ref}}/a_0$	2.75	2.15	2.20, 4.10	1.961, 5.50	2.40
$R_3^{(j),\mathrm{ref}}/a_0$	2.75	2.15	4.10, 2.20	5.50, 1.961	2.40

constant proposed by several authors, such a result has later been found to have been because of an improper sampling of the translational energy in ref 16. The present recalibration of the DMBE potential energy surface (DMBE II) then gave us the possibility of correcting such an error when studying the bimolecular reactions in section 3. Finally, the spectroscopy of the metastable HN_2 species on DMBE II is reported in section 4. For convenience, several energy units have been used: 1 E_h = 219 474.63 cm^{-1} = 627.509 552 kcal mol^{-1}, and 1 a_0 = 0.529 177 211 Å.

2. Potential Energy Surface

According to the DMBE method,[30] the single-valued potential energy surface assumes the form of a cluster expansion, where

$$V^{(n)} = V_{\mathrm{EHF}}^{(n)} + V_{\mathrm{dc}}^{(n)} \tag{1}$$

and $V_{\mathrm{EHF}}^{(n)}$ and $V_{\mathrm{dc}}^{(n)}$ are the n-body extended Hartree−Fock and dynamical correlation energies, respectively. Because of the modularity of DMBE, the recalibration procedure affects only

TABLE 2: Stratified Root-Mean-Squared Deviations (in kcal mol^{-1})

		rmsd	
energy	number of points	DMBE I[a]	DMBE II[b]
20	229	0.152	0.046
40	335	0.337	0.366
60	541	0.654	0.414
80	570	0.753	0.509
100	596	0.815	0.608
120	667	0.905	0.641
140	689	1.005	0.667
160	824	1.049	0.644
200	966	1.151	0.726
500	1046	1.325	0.773
1200	1071	4.087	0.785

[a] Reference 15. [b] This work.

the three-body EHF energy term, and hence we need to consider only this term in the present work (the reader is addressed to ref 15 for other details). Note that, due to a misprint in eq 16 of ref 15, there should be a negative sign in the three-body correlation energy term.

The three-body extended Hartree−Fock energy contribution assumes the distributed-polynomial[31] form

$$V_{\mathrm{EHF}}^{(3)} = \sum_{j=1}^{7} P^{(j)}(Q_1,Q_2,Q_3) \prod_{i=1}^{3} \{1 - \tanh[\gamma_i^{(j)}(R_i - R_i^{j,\mathrm{ref}})]\} \quad (2)$$

where $P^{(j)}$ is the jth polynomial written in terms of Q-coordinates, as defined in eq 22 of ref 15. In this work, we have used two polynomials of sixth-order and one of second-order centered in different C_{2v} geometries and two others of sixth-order plus two of second-order centered at collinear geometries. The least-squares fit has been done as previously[15] but employing now 1074 MRCI/aug-cc-pVQZ energies suitably scaled by the DMBE-SEC method.[25] Extra care has been put on medium and long-range regions of the N−NH channel, as it plays a critical role in the calculation of the rate constant. Table 1 gathers the numerical values of the coefficients in eq 2 for the $HN_2(^2A')$ DMBE II potential energy surface.

The quality of the recalibrated function can be assessed from the stratified root-mean-squared deviations (rmsd's) reported in Table 2. Although chemical accuracy (rmsd $\leq$ 1.0 kcal mol^{-1}) is attained up to 2400 kcal mol^{-1} above the absolute minimum, one should claim only qualitative agreement at high energies because of the many electronic states that may be involved at such regimes and which cannot be accounted for by the single-sheeted function in eq 1. For regions of interest in the HN_2 unimolecular process (up to 40 kcal mol^{-1}), the rmsd is smaller than 0.4 kcal mol^{-1} while for those relevant to study the N + NH reaction (up to 146 kcal mol^{-1}) it is still only 0.7 kcal mol^{-1}. A significant improvement has then been achieved with respect to DMBE I, with the data being probably fitted within the accuracy of the ab initio energies themselves.

A stationary-point analysis has been performed on the DMBE II potential energy surface, with the results being compared with those obtained from other ab initio methods,[12−15] as well as DMBE I,[15] in Tables 3 and 4. For the most important topographical characteristics, the DMBE I[15] and DMBE II functions are seen to be hardly distinguishable, even through the reported normal-mode analysis (the maximum deviation in the calculated vibrational frequencies is 20 cm^{-1}). Such an agreement shows that the distributed-polynomial technique allows a refinement of the previously reported function without severely modifying regions that were considered as properly described by DMBE I. As for the HN_2 decomposition process, the classical barrier is located at 10.6 kcal mol^{-1} above the HN_2 minimum. Although this is slightly lower than the early ab initio value of Walch et al.[11] and the extrapolated result of Walch and Partridge,[13] the agreement with the proposed estimate of Gu et al.[14] (10.0 $\pm$ 1.0 kcal mol^{-1}) is very good. The calculated exothermicity for this process is 4.6 kcal mol^{-1}, in excellent agreement with MRCI calculations[15] and with the Walch and Partridge[13] extrapolated value of 4.3 kcal mol^{-1}. Our result is also only 0.7 kcal mol^{-1} higher than the value reported by Gu et al.[14] using CCSD(T). An interesting feature of the work of Gu et al.[14] is the wrong exothermicity that B3LYP calculations predict. Using the same basis set as CCSD(T), the HN_2 is

TABLE 3: Major Stationary Points of the DMBE II Potential Energy Surface, Compared with the Most Recent Available Data[12−14]

feature	property	KSW[a]	CASSCF/ICCI[b]	CCSD(T)[c]	MRCI[d]	DMBE I[e]	DMBE II[f]
global minimun	R_1/a_0	2.250	2.25	2.223	2.227	2.226	2.226
	R_2/a_0	3.600	3.814	3.588	3.586	3.595	3.595
	R_3/a_0	1.966	2.097	1.985	1.981	1.983	1.983
	ΔV^g/kcal mol^{-1}	3.8	4.31[h]	3.8	4.5	4.5	4.5
	ω_1(N−H)/cm^{-1}	2653			2916	2887	2875
	ω_2(N−N)/cm^{-1}	1826			1818	1862	1842
	ω_3(bend)/cm^{-1}	1047			1118	1086	1096
saddle point for H + N_2 reaction	R_1/a_0	2.139	2.17	2.121	2.124	2.125	2.125
	R_2/a_0	4.190	4.149	4.145	4.135	4.136	4.137
	R_3/a_0	2.703	2.754	2.688	2.685	2.688	2.688
	ΔV^i/kcal, mol^{-1}	11.4	11.34	10.7	10.6	10.6	10.6
	ω_1(N−H)/cm^{-1}	1667i			1619i	1640i	1624i
	ω_2(N−N)/cm^{-1}	1990			2155	2102	2104
	ω_3(bend)/cm^{-1}	749			762	763	778
saddle point for H−N_2 isomerization	R_1/a_0				2.324	2.326	2.326
	R_2/a_0				2.285	2.281	2.281
	R_3/a_0				2.285	2.281	2.281
	ΔV^i/kcal, mol^{-1}				48.5	48.4	48.4
	ω_1(N−H)/cm^{-1}				2676	2753	2753
	ω_2(N−N)/cm^{-1}				1660	1668	1671
	ω_3(bend)/cm^{-1}				2278i	2295i	2275i

[a] Reference 12. [b] Reference 13. [c] Reference 14, considering the aug-cc-p VQZ basis set. [d] Reference 15, fitting a polynomial to a dense grid around each stationary point. [e] Reference 15. [f] This work. [g] Relative to the H + N_2 asymptote. [h] Extrapolated to the basis set limit, see ref 13. [i] Relative to the global minimum.

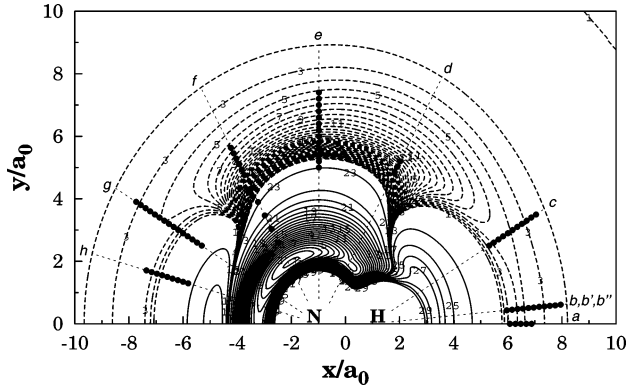

Figure 1. Isoenergy contour plot for the N around a partial relaxed NH molecule, $1.8 \leq R_{NH}/a_0 \leq 2.3$. Solid contours start at -0.355 E_h and equally spaced by 0.01 E_h, while the dashed ones start at -0.134 E_h [N + NH(R_e) energy] with increments of 0.0001 E_h. Shown in solid dots are the newly calculated MRCI ab initio geometries.

TABLE 4: Geometries and Energies of Other Important Stationary Points

	van der Waals			linear TS
property	min H···N_2	min N−H···N	TS N···N−H	N−H−N
R_1/a_0	2.075	7.467	6.846	4.758
R_2/a_0	7.112	1.961	1.965	2.379
R_3/a_0	7.112	5.506	8.811	2.379
E/E_h	−0.3642	−0.1305	−0.1304	−0.0937
ΔV/kcal mol^{-1}	−0.1[a]	−0.2[b]	−0.1[b]	22.9[b]
ω_1(N−H)/cm^{-1}	69	3198	4451	2828i
ω_2(N−N)/cm^{-1}	2337	45	119	567
ω_3(bend)/cm^{-1}	18	16	56i	907

[a] Relative to the H + N_2 asymptote. [b] Relative to the N + NH asymptote.

predicted to be stable by 3.3 kcal mol^{-1} in relation to the H + N_2 asymptote, although the barrier height toward dissociation is close to the predicted value from the present work. As shown in Table 4, the recalibrated DMBE surface predicts also a new NH···N van der Waals minimum lying 0.2 kcal mol^{-1} below the N + NH asymptote. For completeness, we also reported the H···N_2 van der Waals minimum and the linear transition state structures in Table 4.

Because of similarities between the two DMBE potential energy surfaces, except for the N−NH interaction channel, we restrict the discussion to this region. Shown as a contour plot in Figure 1 is a cut of the DMBE II potential energy surface for the N−NH interaction, with the diatomic molecule being partially relaxed. The salient feature is the smaller attractive nature of the entrance region that leads to the HN_2 minimum (cf. Figure 6 of ref 15). Also visible are a collinear NH···N van der Waals minimum and two collinear stationary points: one is the saddle point for NH−N bending leading to isomerization and the other refers to the N···HN van der Waals minimum, which lies bellow the N + NH asymptote by 0.1 kcal mol^{-1} (see also Table 4). A more quantitative assessment of the fit is shown in the two panels of Figure 2, which display one-dimensional cuts (curves a−h) (these are indicated by the dashed lines in Figure 1) for different NH distances and Jacobi angles together with the newly calculated ab initio data. As Figure 2 shows, the new DMBE form describes within a few cm^{-1} the DMBE-SEC corrected MRCI energies. Also relevant is the absence of the spurious collinear barrier that appeared in DMBE I.[15]

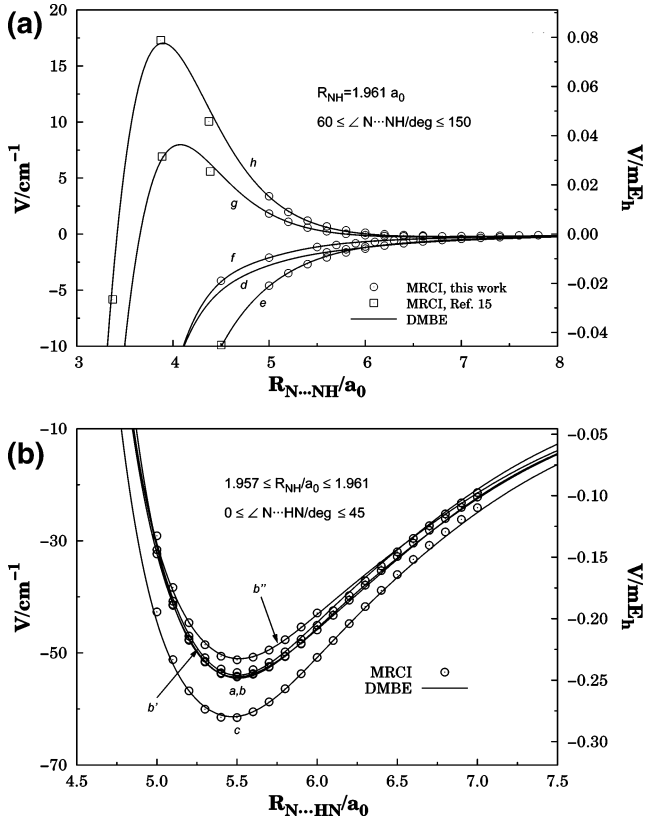

Figure 2. One-dimensional cuts for the long range interaction showing ab initio points calculated in the present work (open dots) and previously calculated (open squares): (a) NH···N and (b) N···NH. The key letters refer to the dotted lines shown in Figure 1.

3. The Reaction N + NH → N_2 + H and Its Reverse

The N + NH → N_2 + H reaction and its reverse are important steps in the combustion of ammonia[32,33] and hydrazine.[21,34] Although the reaction is a simple triatomic reaction, only one direct experimental measurement of the rate constant has been reported[26] by using a quasi-static flash photolysis cell (for room temperature). Indirectly, Whyte and Phillips[28] have studied the NH decomposition produced by N + NH_2 by laser-induced fluorescence, having concluded that the total removal rate constant through reaction with atomic nitrogen is $(7.28 \pm 0.42) \times 10^{13}$ cm^3 mol^{-1} s^{-1}. This value has been subsequently used by Zhan et al.[29] to study the production of NF(b) and IF(B) in the NH_3−F−F_2−CF_3I reaction system. Since Whyte and Phillips[28] report the total removal rate constant, Zhan et al.[29] have used half of this value, giving the same probability to the NH(X) and NH(A) channels. Other crude indirect estimates were reported in the literature[21,27,35] based on simple formalisms. Unfortunately, our previous dynamics calculations[16] were themselves affected by an error in the collision energy sampling, favoring high-energy values. Since DMBE II should be more accurate than DMBE I, only dynamics calculations on the former will be reported.

Following previous work,[16] we have used the QCT method[36] assuming a thermalized ro-vibrational distribution for the NH reactant molecule (see ref 37 for details), with the internal energies (E_{vj}) being determined by solving numerically[38] the time-independent Schrödinger equation and the realistic NH diatomic curve[39] used in modeling both DMBE I and DMBE II. Translational energy sampling employed a Maxwell−Boltzmann distribution for temperatures over the range 100−10 000 K, with 5000 trajectories being integrated for each batch

TABLE 5: Summary of the QCT Results for the N + NH Reaction

		$N_2 + H$		$N + N + H$		$NH + N$	
T/K	b_{max}/Å	N_r	$10^{13}k_1$/cm^3 mol^{-1} s^{-1}	N_r	$10^{13}k_d$/cm^3 mol^{-1} s^{-1}	N_r	$10^{13}k_i$/cm^3 mol^{-1} s^{-1}
100	8.0	1816	3.96 ± 0.07				
300	6.9	1567	4.4 ± 0.1				
500	6.3	1527	4.6 ± 0.1				
1000	5.7	1434	5.0 ± 0.1				
2000	5.2	1304	5.4 ± 0.1				
3000	4.9	1276	5.7 ± 0.1			10	0.04 ± 0.01
4000	4.7	1280	6.1 ± 0.2			26	0.12 ± 0.02
5000	4.6	1271	6.5 ± 0.2	8	0.04 ± 0.01	56	0.29 ± 0.04
6000	4.6	1214	6.8 ± 0.2	24	0.13 ± 0.03	75	0.42 ± 0.05
7000	4.6	1183	7.1 ± 0.2	73	0.44 ± 0.05	99	0.60 ± 0.06
10000	4.6	1024	7.4 ± 0.2	209	1.5 ± 0.1	166	1.20 ± 0.09

using the VENUS96[40] code. Table 5 gathers the calculated rate constants for H + N_2 formation using DMBE II as obtained from

$$k(T) = g_e\left(\frac{8k_BT}{\pi\mu_{N+NH}}\right)^{1/2}\pi b_{max}^2\frac{N_r}{N} \quad (3)$$

where $g_e = {}^1/_6$ and is the electronic degeneracy factor, μ the reduced mass of the colliding species, and k_B the Boltzmann constant. Assuming 68% confidence, the associated error is $\Delta k(T) = k(T)[(N - N_r)/(NN_r)]^{1/2}$.

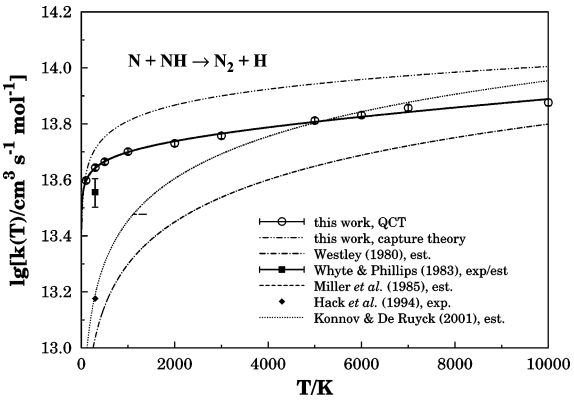

Figure 3. Rate coeffcient for the N_2 + H formation as a function of temperature. The open symbols denote the QCT calculations using DMBE II, while the solid line indicates the Arrhenius fit. Also shown are the classical capture calculations. For comparison we plot estimates from various sources[21,27,29,35] and the experimental value of Hack et al.[26]

Figure 3 shows the calculated rate constant for N_2 formation as a function of temperature. For convenience, the results were fitted to a three-parameter Arrhenius form,

$$k(T) = AT^m\exp(-B/T) \quad (4)$$

leading to the optimum least-squares parameters $A = 4.88 \times 10^{13}$ K^{-m} cm^3 mol^{-1} s^{-1}, $m = -0.094$, and $B = -0.025$ K. The shape of the calculated curve shows a typical capture-type regime for low temperatures, which can be rationalized by the barrierless behavior of the N + NH interaction. Because of this, we may apply capture theory (ref 41 and references therein) to highlight the low-temperature trend of the QCT results.

Consider the spherically averaged long-range interaction for each ro-vibrational combination of N + NH(v,j) to be described by

$$V_{lr}^{vj}(r) = -\langle C_n^{vj}\rangle r^{-n_{vj}} \quad (5)$$

where $\langle C_n^{vj}\rangle$ is the effective long-range coefficient of power n_{vj} and r is the atom−diatom separation. The parameters in eq 5 can then be approximated by a least-squares fit to the long-range spherically averaged potential assuming the NH distance is fixed at the quantum mechanical expectation value of the (v,j) state. The state-specific rate constant assumes the form[42]

$$k_{cap}^{vj}(T) = g_e(T)\frac{2^{(3n_{vj}-4)/2n_{vj}}n_{vj}\pi^{1/2}}{(n_{vj}-2)^{(n_{vj}-2)/n_{vj}}\mu^{1/2}}\Gamma\left(\frac{2n_{vj}-2}{n_{vj}}\right)\times (k_BT)^{(n_{vj}-4)/2n_{vj}}\langle C_n^{vj}\rangle^{2/n_{vj}} \quad (6)$$

with Γ being the gamma function. The total rate coefficient can then be obtained by the usual averaging procedure leading to

$$k_{cap}(T) = Q_{vr}^{-1}(T)\sum_{vj}^{NH}(2j+1)k_{cap}^{vj}(T)\exp\left(-\frac{E_{vj}}{k_BT}\right) \quad (7)$$

where Q_{vr} is the reactants NH ro-vibrational partition function. Figure 3 compares the rate constant predicted by capture theory with our QCT results. Clearly, the reaction obeys a capture-type regime at low temperatures. Because of the high exothermicity, the recrossing value is expected to be small, especially for temperatures up to 300 K or so, and hence will be ignored. Note that for temperatures higher than 3000 K, the capture theory results are only given for qualitative analysis, as the method should no longer be reliable. Note further that for high translational and internal energies resulting from the sampling procedure, the diatomic molecule cannot reorient to find the most favorable attacking geometry, and hence the rate constant becomes nearly temperature-independent. This behavior has been predicted by Miller et al.,[18] with k ($1100 \le T/\text{K} \le 1400$) $= 3 \times 10^{13}$ cm^3 s^{-1} mol^{-1}, our value being about 2.6 times larger. Note that other channels may open at high temperatures, namely, isomerization and total fragmentation; for completeness, these rate constants are also reported in Table 5. Note further that the $T^{0.5}$-dependence proposed by Westley[27] and used recently by Konnov and De Ruyck[20,21] is not verified by the present results.

Also shown in Figure 3 is the experimental data of Hack et al.,[26] $k = 1.5 \times 10^{13}$ cm^3 s^{-1} mol^{-1}, which has been obtained for room temperature. Their result is nearly 3 times lower than our QCT value and the capture-theory result. Even including a crude 20% estimate of possible error,[26] the difference remains substantial. In turn, the agreement with the experimental estimate of Whyte and Phillips[28] is satisfactory. Note, however, that the partition of the total rate of NH removal may not be equal for both electronic states as proposed by Zhan et al.[29] Thus, the observed discrepancies between the calculated and measured rate constants for the title system may be attributed both to

experimental difficulties and to the noninclusion of nonadiabatic effects in the theory as complicated electronic crossings[43,44] are not taken into account by the single-sheeted DMBE II form. Of course, the use of classical mechanics cannot also be excluded as a source of error. However, we emphasize the high quality of the ab initio data and DMBE II fit and the fact that classical mechanical methods work extremely well for rate constant calculations even for the extreme case of three hydrogen atoms.[45] In summary, we can hardly assign the source of discrepancy between the experimental and theoretical results without going beyond the adiabatic picture and/or performing more accurate measurements.

For the H + N_2 endothermic reaction, we have used microreversibility as in previous work.[16] Thus, the H + N_2 formation rate constant assumes the form

$$K(T) = \frac{k_1(T)}{k_{-1}(T)} \tag{8}$$

where k_1 and k_{-1} are the N_2 and NH formation rate constants, respectively. Using the Arrhenius parameters reported[16] for the equilibrium constant, $k_{-1}(T)$ can be expressed by the corresponding coefficients: $A = 1.40 \times 10^{15}$ K^{-m} cm^3 mol^{-1} s^{-1}, $m = -0.10$, and $B = -74\,450$ K. To our knowledge, the only estimate available for comparison is from the GRI-Mech 3.0,[46] which is based on statistical thermodynamical data for the equilibrium constant and the reported k_1 ($T = 298$ K) value of Hack et al.[26] The agreement is seen to be fairly good, although the temperature dependence, also based on eq 8, has been obtained using a single value of the rate constant. We should note that although rate constants for NH + N formation are reported for temperatures down to room temperature, their estimates may suffer from considerable error below 2000 K. Quantitatively, we predict the NH + N rate constant formation to be 4.35 (4.43) $\times 10^{-2}$, 7.27 (6.80) $\times 10^{1}$, and 10.2 (9.1) $\times 10^{3}$ cm^3 s^{-1} mol^{-1} for $T = 2000$, 2500, and 3000 K, respectively, with the values in parentheses being from GRI-Mech.[46]

4. The Reaction N + NH → N_2 + H and Its Reverse

The study of the radical lifetime and $HN_2 \rightarrow N_2$ + H dissociative process using the DMBE II potential energy surface has been carried out as in ref 16 using the complex method.[47,48] Assuming an isolated resonance, the lifetime (τ_n) can be estimated by the associated width (Γ_n) according to the expression $\tau_n = \hbar/\Gamma_n$, while the unimolecular decay of the state is given by $k_n = \Gamma_n/\hbar$. The key elements for the unimolecular decay rate constant and lifetime calculation are the resonance width and the separation between resonances. Our results were obtained using the DVR3D[49] code and Jacobi coordinates: r, the N_2 internuclear distance, R, the atom−diatom separation, and θ, the orientation angle between the vectors **R** and **r**. The primitive DVR basis employed $n_r = 40$, $n_R = 65$, and $n_\theta = 80$, with the parameters of the Morse-like functions being $r_e = 2.3$ a_0, $D_{e,r} = 0.8$ E_h, and $\omega_{e,r} = 0.02$ E_h for the coordinate r, and $R_e = 4.3$ a_0, $D_{e,R} = 0.8$ E_h, and $\omega_{e,R} = 0.01$ E_h for R. The overall process utilized a truncation/diagonalization procedure, resulting in a 3000 dimensional secular problem. The lowest 1000 states have been retained for the complex calculations with the parameters of the negative imaginary potential being varied over the ranges $5.4 \le R_{min}/a_0 \le 5.8$ and $0.004 \le \lambda/E_h \le 0.2$.

Table 6 gathers the energies and widths of the resonances calculated for the DMBE II potential energy surface, together with those previously reported[16] for DMBE I. Also shown for comparison are the results of Li and Guo[50] using double Chebyshev autocorrelation functions based on the KSW potential energy surface. For levels up to 7627 cm^{-1}, the differences with DMBE I are less than 15 cm^{-1}, which shows the similarities between the two surfaces in the region of the HN_2 minimum. We observe as before[16] that our calculated energies are systematically higher than the values reported by Li and Guo[50] and that level splittings due to tunneling are negligible. Such differences can be attributed to small topographical differences between the two surfaces because of the distinct ab initio methods and electronic basis sets employed. Comparing the lifetime for the six leading states of HN_2 reported in Table 6, we conclude that all theoretical predictions are in reasonably good agreement with each other. As anticipated by the structural similarities between the different potential energy surfaces, the HN_2 lifetime is predicted to range from 10^{-9} to 10^{-13} s, in contradiction with the postulated value of 10^{-4} s suggested by kinetic modelers.

TABLE 6: Resonance Parameters for the HN_2 Radical

	Li and Guo[a]		DMBE I[b]		DMBE II[c]	
state	E/cm^{-1}	Γ/cm^{-1}	E/cm^{-1}	Γ/cm^{-1}	E/cm^{-1}	Γ/cm^{-1}
(000)	4045.17	0.0019	4416.3	0.013	4409.1	0.010
(010)	5115.80	0.034	5500.7	0.16	5491.0	0.13
(001)	5766.90	2.09	6187.6	10.6	6172.9	9.1
(020)	6220.55	1.50	6573.0	9.6	6555.4	7.7
(100)	6386.4	55.8	6712	137	6702	134
(011)	6789.8	8.18	7242	35	7224	29
(030)	7289.4	13.5	7627	41	7609	34
(002)	7483.0	56.7	7962	39	7938	37
(021)	7879.6	34.6	8294	73	8273	73
(040)	8312.9	42.3	8655	127	8643	69
(012)	8559.2	79.6	9001	63	8981	60
(003)	9174.4	94.6	9695	96	9680	64

[a] Potential energy surface from ref 12. [b] Potential energy surface from ref 15. [c] This work.

For completeness, we have calculated the unimolecular rate constant $k(T)$ by assuming the high-pressure limit:

$$k(T) = \frac{1}{Q_{HN_2}} \sum_k k_n \exp\left(-\frac{\Delta E_n}{k_B T}\right) \tag{9}$$

where Q_{HN_2} is the HN_2 partition function and $k_n = 1/\tau_n$. The results turn out to be almost indistinguishable from those reported elsewhere[16] and hence will be omitted.

5. Concluding Remarks

A novel (DMBE II) single-sheeted DMBE potential energy surface has been reported for the lowest doublet state of HN_2 by fitting accurate ab initio MRCI energies. As in previous work, such energies have first been corrected semiempirically to account for the basis set/configuration interaction finite sizes by using the DMBE-SEC method. The new fit shows a root-mean-squared deviation much smaller than DMBE I, which is possibly within the accuracy of the fitted ab initio points.

To test the DMBE II potential energy surface, a QCT study of the N + NH exothermic reaction has also been performed. Although it is a simple atom−diatom elementary reaction studied on an accurate potential energy surface, a comparison with the experimental data reported in the literature shows at best fair agreement. Also, the postulated temperature-dependence of $T^{0.5}$ used in previous theoretical models for this reaction could not be confirmed. To investigate the origin of the predicted temperature-dependence at low temperatures, calculations have been performed using classical capture theory and shown to be

in good agreement with the QCT ones. Finally, the resonance states for the metastable HN_2 minima have been found to be in good agreement with those calculated using DMBE I. Further experimental and theoretical work is clearly necessary to clarify the pending issues.

Acknowledgment. This work has the financial support of the European Community (Contract HPRN-CT-2002-00170) and Fundacão para a Ciência e a Tecnologia, Portugal (Contracts POCI/QUI/60501/2004, POCI/AMB/60261/2004, and REEQ/128/QUI/2005).

References and Notes

(1) Hellman, A.; Baerends, E. J.; Biczysko, M.; Bligäard, T.; Christensen, C. H.; Clary, D. C.; Dahl, S.; v.-Harrevelt, R.; Honkala, K.; Jonsson, H.; Kroes, G. J.; Luppi, M.; Manthe, U.; Norskov, J. K.; Olsen, R. A.; Rossmeisl, J.; Skúlason, E.; Tautermann, C. S.; Varandas, A. J. C.; Vincent, J. K. *J. Phys. Chem. B* **2006**, *110*, 17719.

(2) Miller, J. A.; Bowman, C. G. *Prog. Energy Combust. Sci.* **1989**, *15*, 287.

(3) Bozzelli, J. W.; Dean, A. M. *Int. J. Chem. Kinet.* **1995**, *27*, 1097.

(4) Hayhurst, A. N.; Hutchinson, E. M. *Combust. Flame* **1998**, *114*, 274.

(5) Hughes, K. J.; Tomlin, A. S.; Hampartsoumian, E.; Nimmo, W.; Zsély, I. G.; Ujvári, M.; Turányi, T.; Clague, A. R.; Pilling, M. J. *Combust. Flame* **2001**, *124*, 573.

(6) Tomeczek, J.; Gradoń, B. *Combust. Flame* **1998**, *133*, 311.

(7) Hwang, D.; Mebel, A. M. *J. Phys. Chem. A* **2003**, *107*, 2865.

(8) Dickinson, A. S.; Ern, A.; Vesovic, V. *Mol. Phys.* **2005**, *103*, 1895.

(9) Selgren, S. F.; McLaughlin, P. W.; Gellene, G. I. *J. Chem. Phys.* **1989**, *90*, 1624.

(10) Walch, S. P.; Duchovic, R. J.; Rohlfing, C. M. *J. Chem. Phys.* **1989**, *90*, 3230.

(11) Walch, S. P. *J. Chem. Phys.* **1990**, *93*, 2384.

(12) Koizumi, H.; Schatz, G. C.; Walch, S. P. *J. Chem. Phys.* **1991**, *95*, 4130.

(13) Walch, S. P.; Partridge, H. *Chem. Phys. Lett.* **1995**, *233*, 331.

(14) Gu, J.; Xie, Y.; Schaefer, H. F., III *J. Chem. Phys.* **1998**, *108*, 8029.

(15) Poveda, L. A.; Varandas, A. J. C. *J. Phys. Chem.* **2003**, *107*, 7923.

(16) Caridade, P. J. S. B.; Rodrigues, S. P. J.; Sousa, F.; Varandas, A. J. C. *J. Phys. Chem. A* **2005**, *109*, 2356.

(17) Miller, J. A.; Branch, M. C.; Kee, R. J. *Combust. Flame* **1981**, *81*, 43.

(18) Miller, J. A.; Glarborg, P. *Int. J. Chem. Kinet.* **1999**, *31*, 757.

(19) Dean, A. M. *Proceedings of the International Conference on the Foundations of Molecular Modeling and Simulation (FOMMS)*; AIChE Symposium Series, 2001; Vol. 97, p 84.

(20) Konnov, A. A.; De Ruyck, J. *Combust. Sci. Technol.* **2001**, *168*, 1.

(21) Konnov, A. A.; De Ruyck, J. *Combust. Flame* **2001**, *124*, 106.

(22) Werner, H.-J.; Knowles, P. J. *J. Chem. Phys.* **1988**, *89*, 5803.

(23) Dunning, T. H. *J. Chem. Phys.* **1989**, *90*, 1007.

(24) Kendall, R.; Dunning, T., Jr.; Harrison, R. *J. Chem. Phys.* **1992**, *96*, 6769.

(25) Varandas, A. J. C. *J. Chem. Phys.* **1989**, *90*, 4379.

(26) Hack, W.; Wagner, H. G.; Zaspypkin, A. *Ber. Bunsen−Ges.* **1994**, *98*, 156.

(27) Westley, F. *Table of Recommended Rate Constants for Chemical Reactions Occuring in Combustion*; NSRDS-NBS 67; NBS: Washington, DC, 1980.

(28) Whyte, A. R.; Phillips, L. F. *Chem. Phys. Lett.* **1983**, *102*, 451.

(29) Zhang, J.; Huang, R.; Zhuang, Q.; Zhang, C. *Chem. Phys. Lett.* **1990**, *174*, 568.

(30) Varandas, A. J. C. In *Conical Intersections: Electronic Structure, Dynamics & Spectroscopy*; Domcke, W., Yarkony, D. R., Köppel, H., Eds.; Advanced Series in Physical Chemistry; World Scientific: River Edge, NJ, 2004; Chapter 5, p 91.

(31) Martínez-Núnez, E.; Varandas, A. J. C. *J. Phys. Chem. A* **2001**, *105*, 5923.

(32) Kaskan, W. E.; Hughes, D. E. *Combust. Flame* **1973**, *20*, 381.

(33) Skreiberg, O.; Kilpinen, P.; Glarborg, P. *Combust. Flame* **2004**, *136*, 501.

(34) Catoire, L.; Luche, J.; Dupré, G.; Paillard, C. *Shock Waves* **2001**, *11*, 97.

(35) Miller, J. A.; Branch, M. C.; McLean, W. J.; Chandler, D. W.; Smooke, M. D.; Klee, R. J. *Proceedings of the Combustion Institute*; The Combustion Institute: Pittsburgh, PA, 1985; Vol. 20, p 673.

(36) Peslherbe, G. H.; Wang, H.; Hase, W. L. *Adv. Chem. Phys.* **1999**, *105*, 171.

(37) Rodrigues, S. P. J.; Varandas, A. J. C. *J. Phys. Chem. A* **2003**, *107*, 5369.

(38) Leroy, R. J. *A Computer Program for Solving the Radial Schrödinger Equation for Bound and Quasi-Bound Levels*, version 7.5; Chemical Physics Research Report CP-655; University Of Waterloo: Waterloo, Ontario, Canada, 2002.

(39) Varandas, A. J. C.; Silva, J. D. *J. Chem. Soc., Faraday Trans.* **1992**, *88*, 941.

(40) Hase, W. L.; Duchovic, R. J.; Hu, X.; Komornicki, A.; Lim, K. F.; Lu, D.; Peslherbe, G. H.; Swamy, K. N.; Linde, S. R. V.; Varandas, A. J. C.; Wang, H.; Wolf, R. J. *QCPE Bull.* **1996**, *16*, 43.

(41) Varandas, A. J. C. In *Conferencias Plenarias de la XXIII Reunión Bienal de Química*; Feliciano, A. S., Grande, M., Casado, J., Eds.; Universidad de Salamanca: Salamanca, Spain 1991; p 321.

(42) Varandas, A. J. C. *Faraday Discuss. Chem. Soc.* **1987**, *84*, 353.

(43) Walch, S. P. *J. Chem. Phys.* **1991**, *95*, 4277.

(44) Mota, V. C.; Varandas, A. J. C. To be published.

(45) Zhao, M.; Truhlar, D. G.; Blais, N. C.; Schwenke, D. W.; Kouri, D. J. *J. Phys. Chem.* **1990**, *94*, 6696.

(46) Smith, G. P.; Golden, D. M.; Frenklach, M.; Moriarty, N. W.; Eiteneer, B.; Goldenberg, M.; Bowman, C. T.; Hanson, R. K.; Song, S.; Gardiner, W. C., Jr.; Lissianski, V. V.; Qin, Z. http://www.me.berkeley.edu/gri_mech (accessed Oct 2006).

(47) Jolicard, G.; Austin, E. J. *Chem. Phys.* **1986**, *103*, 295.

(48) Jolicard, G.; Leforestier, C.; Austin, E. J. *J. Chem. Phys.* **1988**, *95*, 1026.

(49) Tennyson, J.; Henderson, J. R.; Fulton, N. G. *Comput. Phys. Commun.* **1995**, *86*, 175.

(50) Li, G.; Guo, H. *Chem. Phys. Lett.* **2001**, *347*, 443.